RJC

γ-Fe₂O₃ NANOPARTICLES IMMOBILIZED IN SiO₂ AEROGEL SYNTHESIZED FROM RICE HUSK ASH FOR PHOTO-FENTON LIKE DEGRADATION OF RHODAMINE B

Is Fatimah, Subhi Fadhilah, Yulan and Sherlita Ayu Mawardani

Chemistry Department, Islamic University of Indonesia Kampus Terpadu UII,

Jl. Kaliurang Km 14, Yogyakarta

*E-mail: isfatimah@uii.ac.id

ABSTRACT

Preparation of γ-Fe₂O₃/ SiO₂ aerogel using biogenic silica from rice husk ash (RHA) and the application for photo-Fenton like degradation of rhodamine B (RhB) has been conducted. The synthesis was performed by preparing γ-Fe₂O₃ nanoparticles followed by sol-gel reaction with silica gel extracted from RHA. The physicochemical properties of γ-Fe₂O₃/ SiO₂ aerogel were characterized by x-ray diffraction (XRD), Fourier Transform-Infra Red (FTIR), diffuse reflectance UV-Visible spectrophotometry, gas sorption analyzer and Scanning Electron Microscopy (SEM) analyses. It is shown that the prepared material exhibits the character supporting photocatalytic activity as shown by UV-Vis absorption spectrum. The photocatalytic activity in photo-Fenton like degradation of RhB reveals that γ-Fe₂O₃/ SiO₂ aerogel demonstrate similar degradation rate compared with γ-Fe₂O₃ nanoparticles with the advantageous of its reusability that is maintained stably for three cycles.

Keywords: γ-Fe₂O₃, Biogenic silica, Photo-Fenton like mechanism, Photooxidation.

INTRODUCTION

High concentrations of organic compounds, especially dyestuffs, total suspended solids and high chemical oxygen demand (COD) are the major problems in the processing of textile industry[1,2]. Various methods are considered to be effective in the management of industrial waste, including adsorption, coagulation, electrochemical oxidation, ozonization, photocatalysis and advanced oxidation process (AOP) methods[3,4]. The last two methods are the latest method that is considered effective and environmentally friendly and have high-efficiency value to be applied in the industry. Among several techniques in AOP, photo-Fenton and photo-Fenton like process are considered as the efficient and fast elimination of organic content from water environment over photooxidation mechanism. The oxidation reaction takes place with the presence of catalytically generated hydroxyl (OH •) radicals from oxidants such as hydrogen peroxide. The combination of semiconductor photocatalysts such as TiO_2, ZnO, Fe_2O_3, CdS and ZnS with UV or visible light and even sunlight is one of the advantages of this process to be more economical and reusable. The decomposition of organic compounds through a perfect oxidation process will produce CO_2, H_2O or NH_3 gases that are directly described to the environment so that they do not leave adsorbate and do not require further processing.

As an alternative to TiO_2 photocatalyst that is the most widely known and applied semiconductor, utilization of γ-Fe₂O₃ is an interesting material. With the same photocatalytic mechanism, Fe_2O_3 shows oxidation activity in large dyestuffs. The enhancement of Fe_2O_3 photoactivity was an important effort for increasing photocatalyst performance[5,6]. Within this scheme, some investigations reported the preparation of γ-Fe₂O₃ in the form of nanoparticles and in another mechanism, Fe_2O_3 particles/nanoparticles were preserved in a support-immobilized form. For the second procedure, γ-Fe₂O₃ nanoparticles can be deposited onto either porous or gel materials, one of which was in the form of aerogel γ-Fe₂O₃/SiO₂. The γ-Fe₂O₃/ SiO₂ aerogel can be synthesized through sol-gel reactions with various silica sources such as commercially available silica such as tetra ethyl orthosilicates[7,8]. Principally on some of the principles of

green chemistry and cheap and environmentally friendly photocatalysts, the use of silica sources from plants for synthesis of silica-based or so-called biogenic materials can be applied theoretically[9]. Biogenic silica material will have advantages in terms of the use of recyclable materials. A fundamental study of changes in the structure of the material structure and the change of physicochemical properties during the formation of γ-Fe$_2$O$_3$/SiO$_2$ aerogel may take a role in supporting the development of photooxidation technology applied to the processing of organic contaminant[10,11]. On the other hand, from some literature reported rice husk ash is one of the potential biogenic sources of silica other than some other plants such as grass, corn, and nuts[12,13]. So far, rice husk ash has been reported as the source of silica in silica gel preparation but the study on its utilization in the formation of metal oxide nanoparticles composites especially for γ-Fe$_2$O$_3$/SiO$_2$ aerogel has not been reported yet.

In this paper, photocatalytic activity test of γ-Fe$_2$O$_3$/SiO$_2$ material was tested for rhodamine B. The selection of rhodamine B as the model is due to its abundantly and widely utilized for such textile and paint industries. Its toxicity and carcinogenicity towards human and biological elements in the environment are the important factors concerning for degradation study[14,15].

EXPERIMENTAL

Materials
Rice husk was obtained from the agricultural area in Sleman District, Special Region of Yogyakarta, Indonesia. The ash from rice husk (RHA) was obtained by calcination the rice husk at the temperature of 700º C for 3h. Some chemicals consist of NaOH, HCl, FeCl$_3$, ammonium hydroxide and rhodamine B were purchased from merk-Millipore, Germany and used as received.

Silica extraction from RHA
Silica extraction from RHA was performed by refluxing RHA in NaOH 4M for 4 h. The filtrate from reflux solution was washed with distilled water, filtered, and then slow titrated with HCl 2M. The mentioned process produced a gel at the pH of 8. The gel was filtered, washed with distilled water till free from chloride ions, and the gel was dried in an oven at 60ºC. The obtained gel is silica gel.

Synthesis of γ-Fe$_2$O$_3$/SiO$_2$
The synthesis of γ-Fe$_2$O$_3$/SiO$_2$ using silica gel derived from RHA was conducted by firstly prepare γ-Fe$_2$O$_3$ nanoparticles. The preparation was performed by mixing FeCl$_3$·6H$_2$O and FeSO$_4$·7H$_2$O (molar ratio Fe^{3+}: Fe^{2+} = 3:2) dissolved in 25 ml distilled water. The solution of γ-Fe$_2$O$_3$ nanoparticles was analyzed by particle size analyzer using HORIBA-X, HORIBA Scientific (Kyoto, Japan) instrument. The nanoparticles solution was then mixed with the silica gel under reflux for 2 h. Theoretic Fe content in the mixture was 15% which was calculated based on silica content in the silica gel. An NH$_4$OH (3,5 M) solution was added dropwise into the mixture to increase pH until 11. After aging for 3 h, the product was then dried at 60°C. In order to compare the Fe$_2$O$_3$ phase in the synthesis, the similar procedure was conducted to produce Fe$_2$O$_3$ without the addition of silica gel in the mixture.

Characterization
The character of the material was performed by x-ray diffraction (XRD), gas sorption analyzer, scanning electron microscope-energy dispersive X-ray (SEM-EDX). XRD patterns for materials were recorded using Shimadzu X6000 X-ray diffractometer with a Cu Kα (40 kV, 45 mA). The scans were performed at the range of 3-80º in steps of 0.004º. Gas sorption analyzer of Quantachrome instrument was utilized for adsorption-desorption isotherm (BET method), specific surface area, pore volume and pore radius.

RESULTS AND DISCUSSION
In principle, the preparation of γ-Fe$_2$O$_3$/SiO$_2$ was started from the formation of Fe$_2$O$_3$ nanoparticles followed by sol-gel interaction between the nanoparticles and silica gel obtained from RHA extraction.

The preparation of nanoparticles was conducted using general method reported from previous works[16,17]. In order to ensure that the prepared Fe_2O_3 is in nanoparticle form, the particle size analysis using dynamic scattering method was performed. The distribution of Fe_2O_3 is presented in Fig.-1. It is confirmed that the particles are available in nanosize with the mean diameter of 60nm.
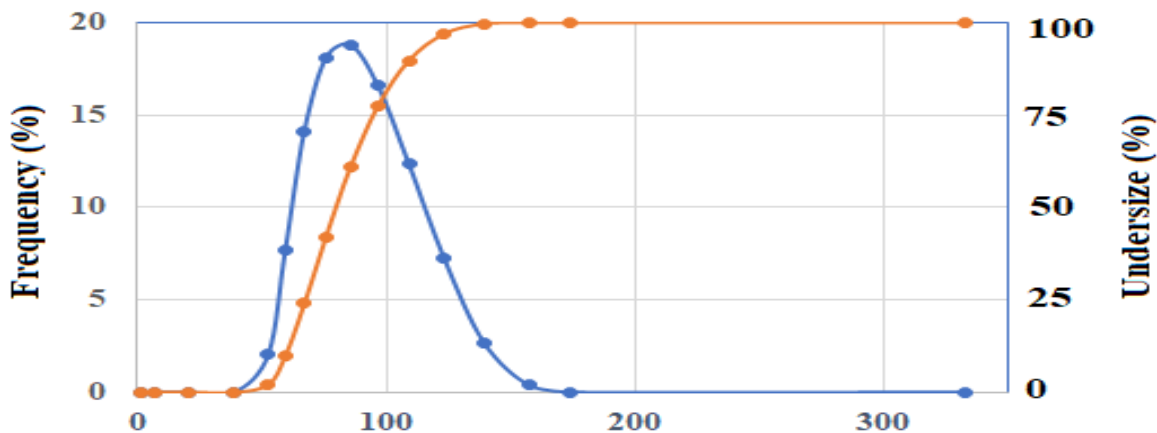

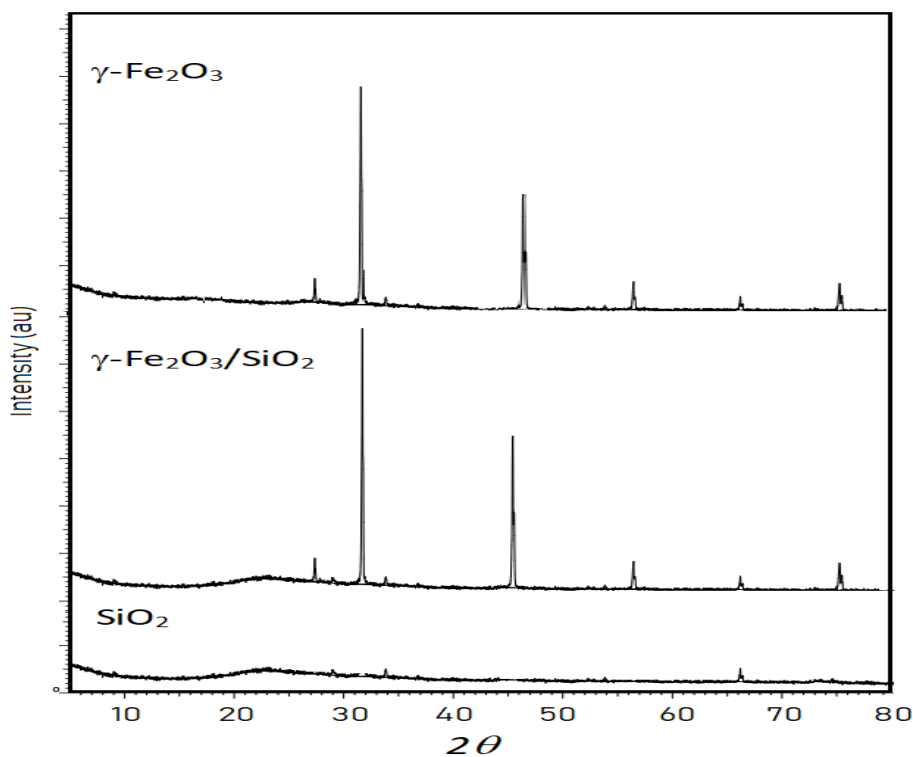Fig.-1: Particle size distribution of γ-Fe_2O_3 nanoparticles

Fig.-2: XRD pattern of materials

The result of XRD analyses to the prepared γ-Fe_2O_3 nanoparticles and γ-Fe_2O_3/SiO_2 show peaks corresponding to the standard data for γ-Fe_2O_3 (JCPDS no. 89.0691) (Fig. 2). The characteristic diffraction peaks of the synthesized γ-Fe_2O_3 seen in $2\theta(°)$ = 26.11; 32.172; 33.928; 43.472; 53.886; 57.116 and 65,185°. By using Scherer formula:

$$L = \frac{K\lambda}{B\cos\theta} \tag{1}$$

With B = full width at half maximum, K = Scherer constant, usually 0.89, λ= wavelength of radiation, and θ= reflection angle, it is found that crystallite size of γ-Fe$_2$O$_3$ in bulk and γ-Fe$_2$O$_3$/SiO$_2$ forms are 1.45nm and 1.39 nm respectively. Compared to other in-situ prepared Fe$_2$O$_3$, the obtained γ-Fe$_2$O$_3$/SiO$_2$ material indicates the formation of a high crystalline, for example, synthesis of γ-Fe$_2$O$_3$/SiO$_2$ reported by Zhang et al., (2014). The immobilization of γ-Fe$_2$O$_3$ was also reflected by the change of surface morphology as depicted by SEM profile in Fig. 3. Compared to SiO$_2$, γ-Fe$_2$O$_3$/SiO$_2$ demonstrates the rougher surface as an indication of aerogel aggregation formed. The formation of aggregates is generally obtained in the aerogel composite as reported by the previous works[19,7,20].EDX spectra of SiO$_2$ and γ-Fe$_2$O$_3$/SiO$_2$ materials confirm that SiO$_2$ obtained from RHA contains silica as a major component (68.79% wt.) and other metals such as Al, Fe, and Na as minor components. The EDX analysis also notified that Fe content in γ-Fe$_2$O$_3$/SiO$_2$ is about 13.88% wt.
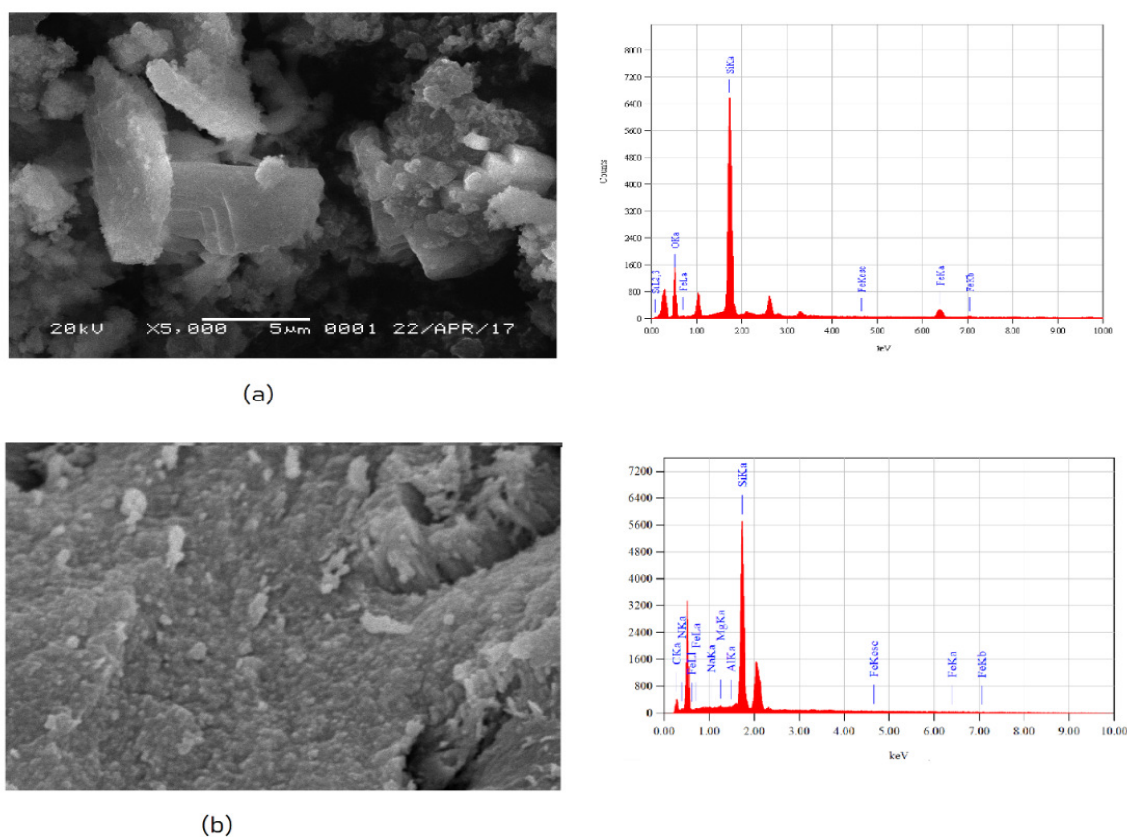

(a)

(b)

Fig.-3: SEM-EDX profile of (a) γ-Fe$_2$O$_3$/SiO$_2$ (b) SiO$_2$

Figure-4 shows the FTIR spectra of SiO$_2$, γ-Fe$_2$O$_3$ and γ-Fe$_2$O$_3$/SiO$_2$ samples. SiO$_2$ and γ-Fe$_2$O$_3$/SiO$_2$ exhibit some peaks as a reflection of the Si-O bond at 1100 to 1000 cm^{-1}. The bands are in also related to the stretching vibrations of the Si–O bond at 800 and 470 cm^{-1}. Meanwhile, γ-Fe$_2$O$_3$ and γ-Fe$_2$O$_3$/SiO$_2$ demonstrate the absorption spectra at 700, 637 and 563 cm^{-1} that are assigned to the Fe–O bond of theγ-Fe$_2$O$_3$ phase. By comparing the spectra of SiO$_2$ and γ-Fe$_2$O$_3$/SiO$_2$, it is revealed that the bands correspond to Si-O bond is found at higher wavenumber for γ-Fe$_2$O$_3$/SiO$_2$, means that there is an increasing vibration energy caused by the interaction of Fe with Si.

Figure-5 presents optical absorption profiles of the SiO$_2$ and γ-Fe$_2$O$_3$/SiO$_2$. The spectrum of γ-Fe$_2$O$_3$/SiO$_2$ demonstrated absorption peaks at around 380nm and at the range of 400-500nm. The bands are related to the electron transmission from the presence of Fe-O bond and the electronic absorption by γ-Fe$_2$O$_3$

547

structure. Meanwhile, SiO_2 expresses the absorption band at the UV range and does not give any absorption at visible range. This result is similar with the previous investigation on the preparation of α-Fe_2O_3/SiO_2 [21].

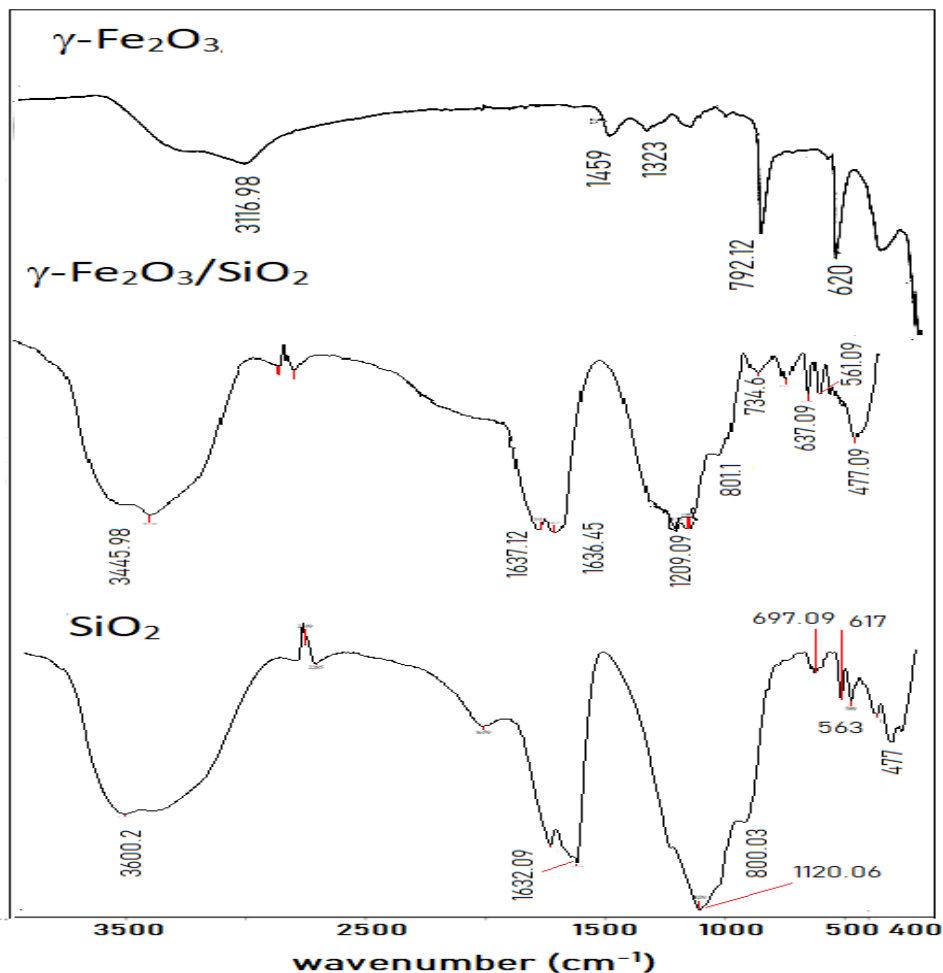Fig.-4: FTIR spectra of SiO_2, γ-Fe_2O_3, and γ-Fe_2O_3/SiO_2 samples

In order to investigate the pore size and the specific surface area, gas sorption analyzer was conducted. Fig.-6 shows the N_2 adsorption/desorption isotherm of SiO_2 and γ-Fe_2O_3/SiO_2. Both materials do not adsorb the N_2 molecule at low P/Po and it is reflecting type IV of the adsorption/desorption isotherm. The pattern is characteristic for typical of the combination of microporous and mesoporous material. Small increasing adsorption capability of γ-Fe_2O_3/SiO_2 is identified and it is represented by the higher specific surface area and pore volume parameters compared to SiO_2 listed in Table-1. From the pore distribution curve, it is also seen that γ-Fe_2O_3/SiO_2 exhibits the formation of pores with the bigger radius corresponding to the increasing adsorption capability.

Table-1: Surface parameter of γ-Fe_2O_3/SiO_2 and SiO_2

Parameter	γ-Fe_2O_3/SiO_2	SiO_2
Specific surface area (m^2/g)	64.89	60.06
Pore volume (cc/g)	0.181	0.164
Pore radius (nm)	6.8	6.9
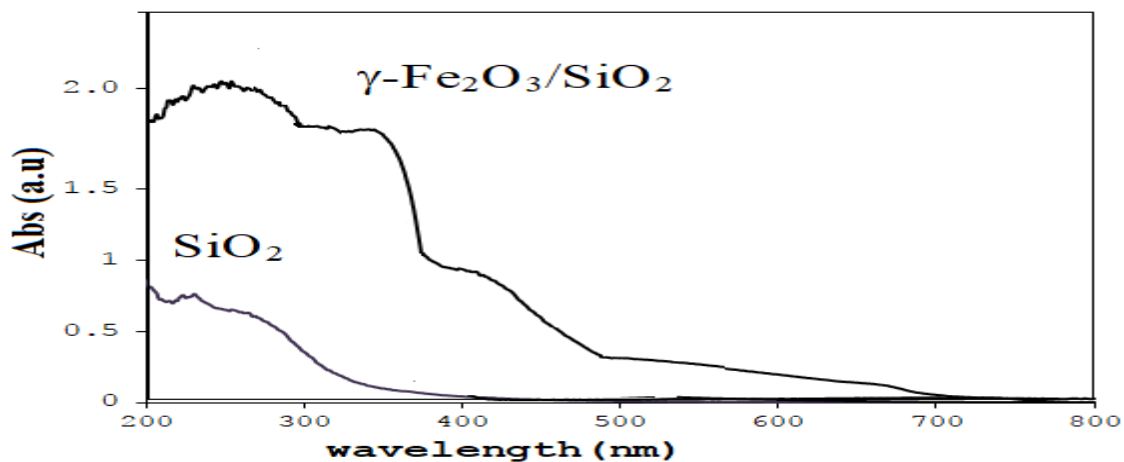
Fig.-5: Optical absorption profiles of the SiO$_2$ and γ-Fe$_2$O$_3$/SiO$_2$
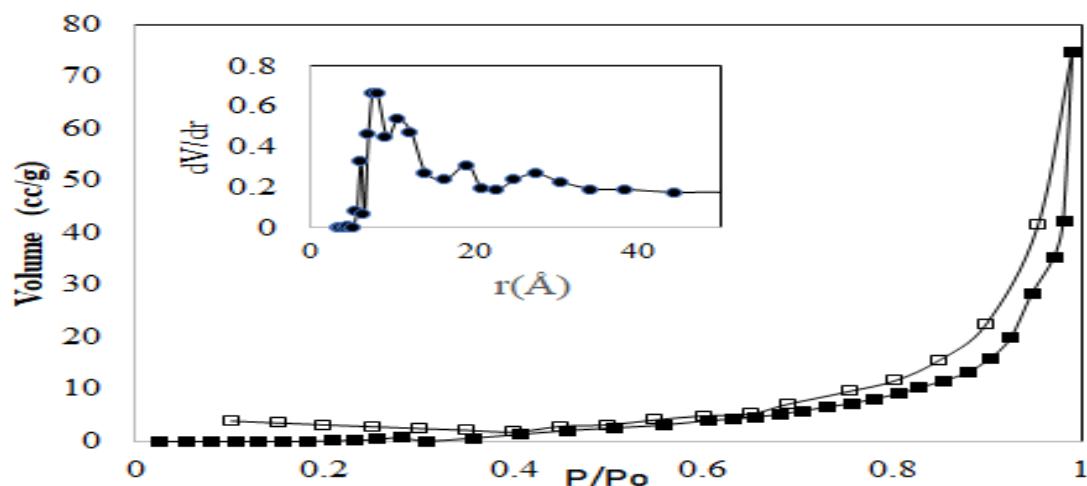
(a)
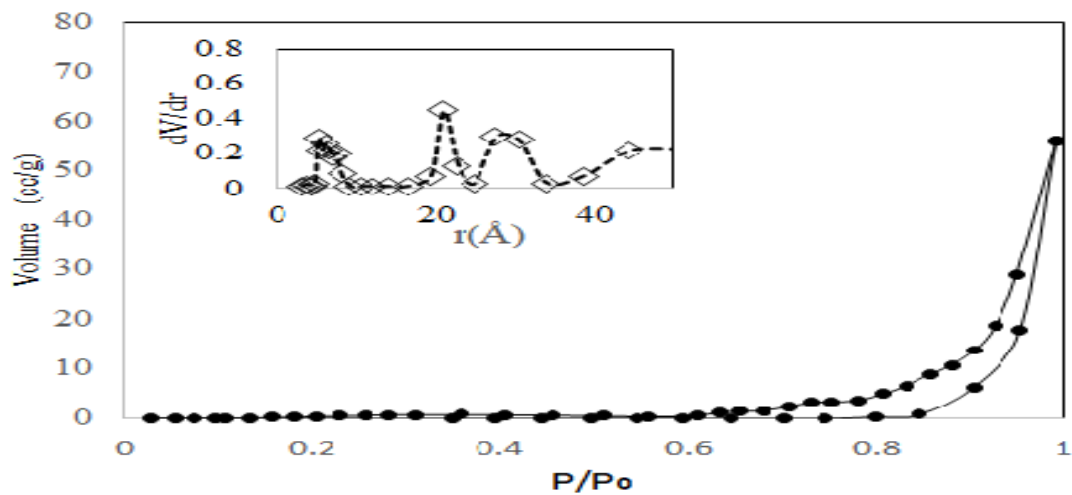
(b)

Fig.-6: N$_2$ adsorption/desorption isotherm of γ-Fe$_2$O$_3$/SiO$_2$ (a) and SiO$_2$ (b)

γ-Fe$_2$O$_3$ NANOPARTICLES IMMOBILIZED IN SiO$_2$ AEROGEL   Is Fatimah *et al.*
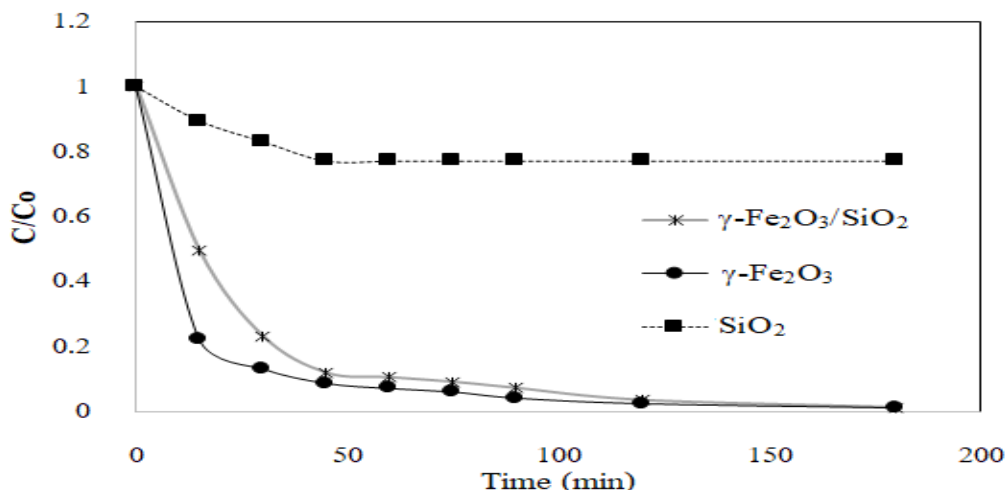
Fig.-7: Kinetics of RhB photooxidation over γ-Fe$_2$O$_3$/SiO$_2$, γ-Fe$_2$O$_3$ and SiO$_2$

Photocatalytic activity of γ-Fe$_2$O$_3$/SiO$_2$ was tested in RhB photodegradation. The photocatalytic activity as also evaluated over varied system: adsorption, photocatalysis and photooxidation. Adsorption experiment was set up by the addition of photocatalyst without UV Lamp exposure while photocatalysis and photooxidation experiments were conducted by the addition of both photocatalyst and UV Lamp exposure with and without H$_2$O$_2$ addition as the oxidant, respectively. Kinetics of RhB photooxidation over γ-Fe$_2$O$_3$/SiO$_2$ compared with the utilization of γ-Fe$_2$O$_3$ and SiO$_2$ is depicted in Fig.-7 and calculated rate and kinetic constant presented in Table-2. Evaluation of the kinetics was performed by two kinetics model with the following equation:
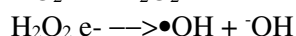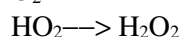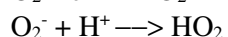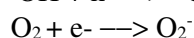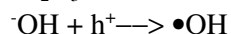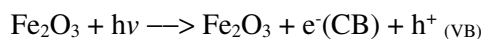
Pseudo-First Order Kinetic equation:
$$\ln \frac{C}{Co} = -kt \qquad (2)$$

and
Pseudo-Second Order Kinetic equation:
$$\frac{1}{C_t} - \frac{1}{C_o} = kt \qquad (3)$$

Where Co and C are RhB initial concentration and concentration at certain time *t*, k is kinetics constant and t is a time of reaction/treatment[22]. The photooxidation reactions over both γ-Fe$_2$O$_3$ and γ-Fe$_2$O$_3$/SiO$_2$ obey first-order kinetic, and from the kinetics data, it can be concluded that γ-Fe$_2$O$_3$ gives fastest RhB reduction meant that γ-Fe$_2$O$_3$ has the highest photocatalytic activity. Meanwhile, compared to that of the utilization of γ-Fe$_2$O$_3$, the kinetics of RhB reduction over γ-Fe$_2$O$_3$/SiO$_2$ is slightly lower but it gives the similar value of initial rate as well as kinetics constant. The lower reaction rate is related to the amount of photoactive material in the photocatalyst, in this case the amount of γ-Fe$_2$O$_3$. Due to the photocatalysis mechanism, the higher surface active will lead to the rapid formation of radicals for oxidizing RhB as a target molecule. The possible mechanism is as follow:

Fe$_2$O$_3$ + hv —> Fe$_2$O$_3$ + e$^-$(CB) + h$^+$ $_{(VB)}$
$^-$OH + h$^+$—> •OH
O$_2$ + e- —> O$_2$$^-$
O$_2$$^-$ + H$^+$ —> HO$_2$
HO$_2$—> H$_2$O$_2$
H$_2$O$_2$ e- —>•OH + $^-$OH

As there is an interaction between UV light (hν) with photoactive species (Fe$_2$O$_3$), the formation of radicals occurred. The produced radicals have potency for organic molecule degradation over oxidation mechanism. From the trend, it is also seen that the concentration reduction is in the similar values after the time of treatment for more than 60 minutes. The kinetic curve in Fig.-8 suggests that there is significant RhB degradation rate over photocatalysis and photooxidation treatment compared to adsorption by following the order of reaction rate: photooxidation > photocatalysis > adsorption. The comparison also reveals that the similar degradation rate achieved by γ-Fe$_2$O$_3$/SiO$_2$ in the smaller amount γ-Fe$_2$O$_3$ as photoactive material.
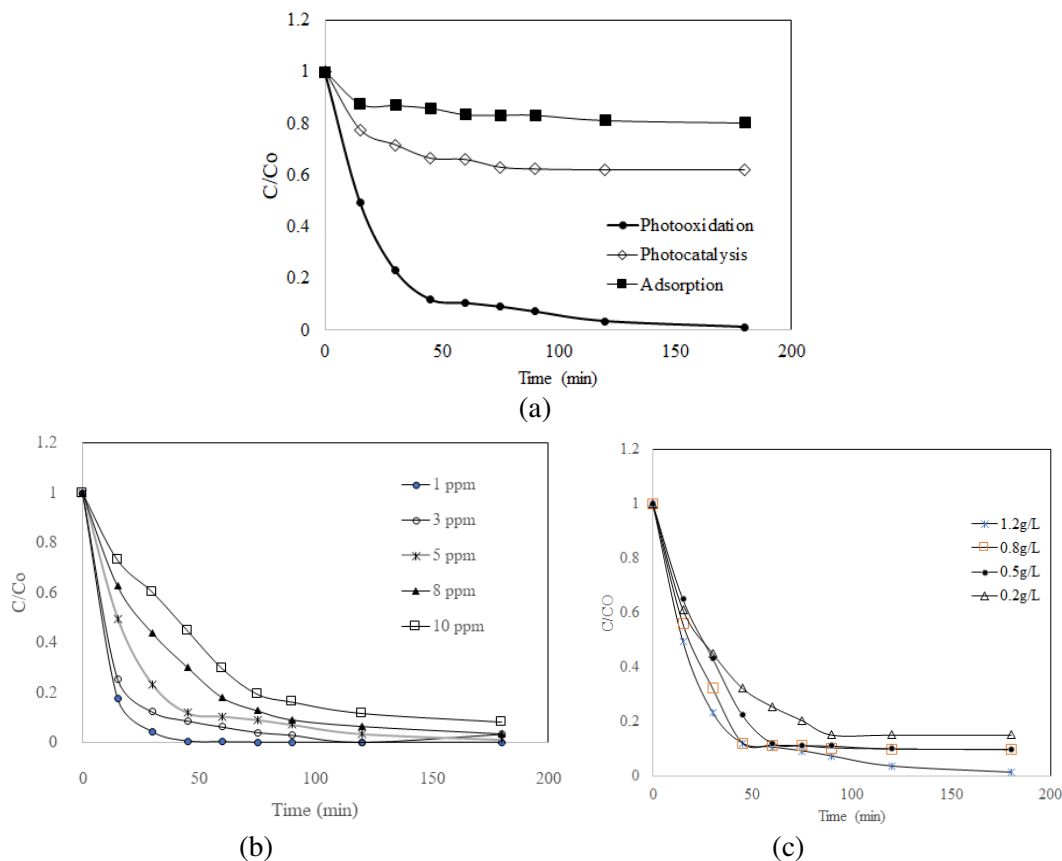

(a)

(b)

(c)

Fig.-8: (a) Comparison of kinetic RhB photo-Fenton like degradation by varied mechanism ([RhB]:5 ppm, catalyst : 0.8 g/L) (b) Kinetic RhB photo-Fenton like degradation over γ-Fe$_2$O$_3$/SiO$_2$ at varied RhB concentration (catalyst : 0.8 g/L) (c) Effect of γ-Fe$_2$O$_3$/SiO$_2$ catalyst dosage on RhB photo-Fenton like degradation ([RhB]: 5 ppm)

Table-2: Kinetics parameter of RhB degradation over photo-Fenton like oxidation under varied catalysts and condition

Photocatalyst	[RhB]/ ppm	Catalyst dosage (g/L)	Initial rate (ppm/min)	Order of reaction (R^2 of simulation)	k/ min^{-1}
SiO$_2$	5	0.8	1.09 x10^{-2}	nd	5.6x10^{-4}
γ-Fe$_2$O$_3$	5	0.8	7.73x10^{-2}	1 (0.9956)	2.12x10^{-2}
γ-Fe$_2$O$_3$/SiO$_2$	1	0.8	1.66 x10^{-2}	1 (0.9967)	4.4x10^{-2}
γ-Fe$_2$O$_3$/SiO$_2$	3	0.8	4.69 x10^{-2}	1 (0.9867)	3.55 x10^{-2}
γ-Fe$_2$O$_3$/SiO$_2$	5	0.2	6.21 x10^{-2}	1 (0.9972)	2.02 x10^{-}
γ-Fe$_2$O$_3$/SiO$_2$	5	0.5	7.33 x10^{-2}	1 (0.9895)	2.71 x10^{-}
γ-Fe$_2$O$_3$/SiO$_2$	5	0.8	7.45 x10^{-2}	1 (0.9972)	2.88 x10^{-2}
γ-Fe$_2$O$_3$/SiO$_2$	5	1.2	7.45 x10^{-2}	1 (0.9855)	2.88 x10^{-2}
γ-Fe$_2$O$_3$/SiO$_2$	10	0.8	1.17 x10^{-2}	1 (0.9907)	2.12 x10^{-2}

γ-Fe$_2$O$_3$ NANOPARTICLES IMMOBILIZED IN SiO$_2$ AEROGEL

Is Fatimah *et al.*

The trend revealed that γ-Fe$_2$O$_3$/SiO$_2$ plays a role as photocatalyst by catching the photon to produce active reactant for RhB degradation. The oxidation comes from the electronic transition in the electronic band level of the γ-Fe$_2$O$_3$ semiconductor. In addition, the presence of oxidant accelerates the formation of hydroxy radicals from either the H$_2$O$_2$ cleavage or radical/ super radical formation from the interaction between semiconductor photocatalyst and H$_2$O$_2$. The increasing reaction rate achieved as increasing photocatalyst dosage and get optimum condition at the addition of 0.8g/L. The higher dosage of photocatalyst generates solution turbidity that is affecting to reduce light penetration into solution.

As an advantage of γ-Fe$_2$O$_3$/SiO$_2$, the reusability of the photocatalyst is demonstrated by comparing kinetics from the first usage until the third usage in Fig.-9. From the kinetic curves, it is concluded that the γ-Fe$_2$O$_3$/SiO$_2$ maintains a stable photoactivity from first until the third cycle. This condition could not be achieved by utilization of the bulk γ-Fe$_2$O$_3$ since it could not be recovered after utilization.
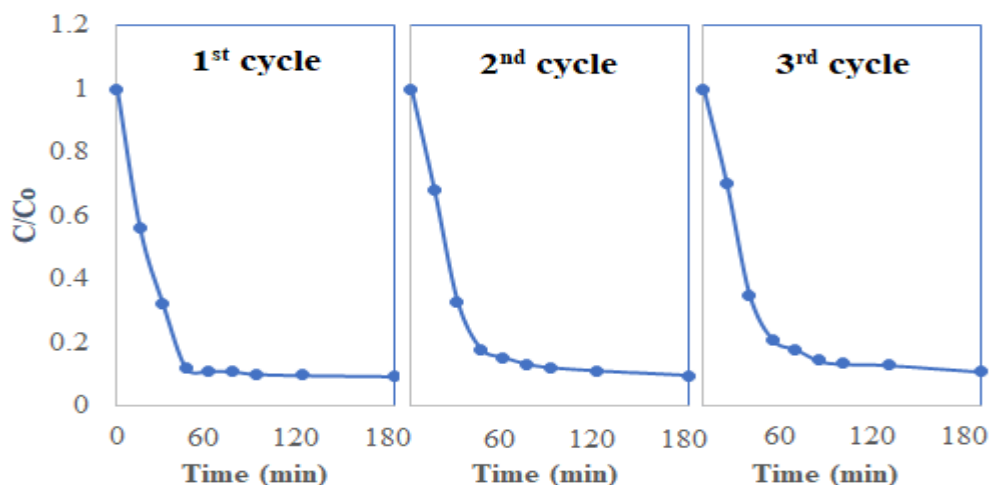

Fig.-9: Kinetics of RhB degradation over γ-Fe$_2$O$_3$/SiO$_2$ for first to the third cycle

CONCLUSION

γ-Fe$_2$O$_3$/SiO$_2$ was successfully produced using silica from rice husk ash. The material has photoactivity as shown by the capability for degradation of rhodamine B photooxidation over photo-Fenton like mechanism. The reactions obey pseudo 1st order reaction with the similar activity compared to γ-Fe$_2$O$_3$. Prepared photocatalyst exhibits reusability as shown by stably reaction rate until the 3rd cycle of usage.

REFERENCES

1. N. Sharma, D.P. Tiwari, and S.K. Singh, *Rasayan Journal of Chemistry*, **7**, 399 (2014).
2. P. Thamilarasu, M. Mohan, V. Dharmalingam, R. Sharmila, and K. Karunakaran, *Rasayan Journal of Chemistry*, **7**, 390 (2014).
3. J. Herrmann, C. Duchamp, M. Karkmaz, B.T. Hoai, H. Lachheb, E. Puzenat, and C. Guillard, J*ournal of Hazardous Materials*, **146**, 624 (2007), **DOI**: 10.1016/j.jhazmat.2007.04.095.
4. M.A. Quiroz, E.R. Bandala, and C.A. Martínez-huitle, In *Pesticides - Formulations, Effects, Fate* . (2007), **DOI:** 10.5772/13597.
5. S.S. Shinde, C.H. Bhosale, and K.Y. Rajpure, J*ournal of Molecular Catalysis A: Chemical* **347**, 65 (2011), **DOI:** 10.1016/j.molcata.2011.07.012.
6. M.A. Mahadik, S.S. Shinde, K.Y. Rajpure, and C.H. Bhosale, *Materials Research Bulletin*, **48**, 4058 (2013), **DOI:** 10.1016/j.materresbull.2013.06.031
7. D. Niznansky, N. Viart, and J.L. Rehspringer, *Journal of Sol-Gel Science and Technology*, **8**, 615 (1997), **DOI:** 10.1007/BF02436910
8. T. Meng, P. Xie, H. Qin, H. Liu, W. Hua, X. Li, and Z. Ma, *Journal of Molecular Catalysis A:*

552

Chemical **, 421**, 109 (2016), **DOI:**10.1016/j.molcata.2016.05.017.

9. P. Saraswathi and M. Makeswari, *Rasayan Journal of Chemistry*, **10**, 759 (2017).

10. A. Tadjarodi, M. Haghverdi, and V. Mohammadi, *Materials Research Bulletin*, **47**, 2584 (2012), **DOI:** 10.1016/j.materresbull.2012.04.143.

11. C.H. and Y.Q. Hexin Zhang, in *Advances in Nanocomposites - Synthesis, Characterization and Industrial Applications* (2011), pp. 40–60, **DOI:** 10.5772/604.

12. Ashish Dat, *Thesis*, Department of Chemistry, University of Iowa, Iowa. (2012).

13. S. Sankar, S.K. Sharma, and D.Y. Kim, *An International Journal of Engineering Sciences,* **16**, 353 (2016).

14. R. Nagaraja, N. Kottam, C.R. Girija, and B.M. Nagabhushana, *Powder Technology*, **215**–**216**, 91 (2012), **DOI:** 10.1016/j.powtec.2011.09.014.

15. Q.I. Rahman, M. Ahmad, S.K. Misra, and M. Lohani, *Materials Letters*, **91**,170 (2013), **DOI:**10.1016/j.matlet.2012.09.044.

16. J. Grabis, G. Heidemane, and D. Rašmane, *Materials Science (Medžiagotyra)*, **14**, 1392 (2008), **DOI:** 10.1.1.475.580.

17. S. Chakrabarti, S.K. Mandal, B.K. Nath, D. Das, D. Ganguli, and S. Chaudhuri, *The European Physical Journal B - Condensed Matter* **,34**, 163 (2003), **DOI:** 10.1140/epjb/e2003-00208-2.

18. X. Zhang, Y. Niu, Y. Yang, Y. Li, and J. Zhao, *New Journal of Chemistry*, **38**, 4351 (2014), **DOI:** 10.1039/C4NJ00389F.

19. I. Saikia, M. Hazarika, M. Bordoloi, and C. Tamuly, *Journal of Bionanoscience*, **11**, 203 (2017), **DOI:** 10.1166/jbns.2017.1436.

20. J.S. Lee, E.J. Lee, and H.J. Hwang, *Transactions of Nonferrous Metals Society of China (English Edition)*, **22**, s702 (2012), **DOI:** 10.1016/S1003-6326(12)61790-7

21. K. Uma, N. Arjun, G.T. Pan, and T.C.K. Yang, *Applied Surface Science*, **425**, 377 (2017), **DOI:**10.1016/j.apsusc.2017.06.300

22. A. Mohammadi, *Progress Color*, *Colorants and Coating,* **9**, 247 (2016).

[RJC-2087/2018]